ISSN: 1231-4005
e-ISSN: 2354-0133
DOI: 10.5604/12314005.1213554

DETERMINATION OF WATER COLLECTION ON TWO- AND THREE-DIMENSIONAL AERODYNAMIC SURFACES IN EXTERNAL TWO-PHASE FLOW IN ATMOSPHERIC CONDITIONS

Janusz Sznajder

Institute of Aviation, Department of Aerodynamics
Krakowska Avenue 110/114, 02-256 Warsaw, Poland
tel.:+48 8460011, ext. 492, fax: +48 8464432
e-mail: janusz.sznajder@ilot.edu.pl

Abstract

Simulations of two-phase flow cases consisting of air and water dispersed in atmosphere were conducted using ANSYS FLUENT solver. The computational model was built with the aim of determination of zones of water droplets impinging on the investigated surface, which is a first step towards simulations of ice accretion in flow conditions where super cooled water is present as dispersed phase. It follows Eulerian approach, currently most effective approach for determination of distribution of water collection on two- and three-dimensional surfaces. Dispersed water is treated as continuous phase and its transport equations are being solved along with air flow equations in the whole computational domain. There are two specific factors of this two-phase flow problem. One of them is ratio of air and water density, which is a cause of existence of two time scales in obtaining a numerical solution of this problem: one for convergence of air flow solution and another for solution of flow of dispersed water in the computational domain. This required development of a specific strategy in obtaining a numerical solution in some circumstances important in aerodynamics, especially at high angle of attack with flow recirculation zones on the wing. The other factor is relatively low concentration of water droplets in conditions important for atmospheric icing. The consequence of this is possibility of uncoupling of solution for both phases and narrowing the solution of the phase of dispersed water to a small region of non-uniformity of velocities of the dispersed phase. Results for two objects: an airfoil and helicopter tail rotor blade, exploiting the developed computational strategy will be presented.

Keywords*: flow simulations, aerodynamics, two-phase flow, simulations of ice accretion, Aircraft Engineering, Transport, Vehicles*

1. Introduction

Determination of flow field of dispersed water around aircraft surface is a first step towards finding zones of impacting droplets, which, depending on air temperature, may freeze on unheated surface leading to deterioration of aerodynamic characteristics or of lifting and control surfaces, engine inlets or failure of sensors of flight parameters exposed to external flow. Currently the most effective approach for solution of the flow of dispersed water droplets is Eulerian approach where dispersed water is treated as continuous phase and equations describing droplet flow are being solved alongside equations of air flow in the same points of computational domain. This approach allows finding zones of local concentrations of the dispersed water around aircraft surface and in the impact zones on the surface. This approach is an alternative to Lagrangian approach involving integration of equations of motion of individual droplets, which would involve large computational efforts particularly in three-dimensional flow. Examples of solutions presented in this paper were obtained using a computational model created for treatment of problems involving contact of droplets with the aircraft surface.

2. Flow model

The dispersed water is treated as continuous phase, and its motion is described by equations of conservation of mass and momentum [1, 2]:

$$\frac{\partial \rho_d}{\partial t} + \nabla \cdot \rho_d \overrightarrow{U_d} = 0, \tag{1}$$

$$\frac{\partial}{\partial t}\left(\rho_d \overrightarrow{U_d}\right) + \nabla \cdot \left(\rho_d \overrightarrow{U_d}\right)\vec{U}_d = \overrightarrow{f_d} + \rho_d \left(1 - \frac{\rho_a}{\rho_w}\right)\vec{g} - \frac{\rho_d}{\rho_w} \cdot \nabla p, \tag{2}$$

where:

$\overrightarrow{f_d}$ – aerodynamic force acting on unit volume of the water phase,

$$\overrightarrow{f_d} = \frac{3}{4} \cdot \frac{c_D}{d} \cdot \frac{\rho_a}{\rho_w} \cdot \rho_d \left|\vec{U}_a - \vec{U}_d\right|\left(\vec{U}_a - \vec{U}_d\right), \tag{3}$$

d – droplet diameter,

$\vec{g}$ – gravitational acceleration,

p – static air pressure,

$\overrightarrow{U_a}$ – local velocity of the air,

$\overrightarrow{U_d}$ – local velocity of the dispersed water phase,

t – time,

ρ_a – air density,

ρ_d – local density of the dispersed water phase,

ρ_w – water density.

Force $\overrightarrow{f_d}$ is aerodynamic drag force acting on unit volume of the water phase, evaluated based on drag of single water droplet, which is a function of Reynolds number. Commonly the circular-shape approximation is used in evaluation its value. In the presented work, the equation proposed by Morrison [3], adequate in the wide range of Reynolds numbers was applied:

$$c_D = \frac{24}{\mathrm{Re}} + \frac{2.6 \cdot \frac{\mathrm{Re}}{5}}{1 + \left(\frac{\mathrm{Re}}{5}\right)^{1.52}} + \frac{0.411\left(\frac{\mathrm{Re}}{263000}\right)^{-7.94}}{1 + \left(\frac{\mathrm{Re}}{263000}\right)^{-8}} + \left(\frac{\mathrm{Re}^{0.8}}{461000}\right), \tag{4}$$

where c_D is non-dimensional coefficient of drag.

The second term in equation (2) represents sum of buoyance and weight and the last term is pressure force due to pressure gradient in the vicinity of the surface of the object.

Equations (1)-(4) were implemented in the ANSYS FLUENT solver using the system of User-Defined Scalars, which allows for solution of transport equations for the variables represented as User-Defined Scalars (UDSs). In the described model for UDSs were used: one for density of the dispersed phase ρ_d and three for components of droplet velocity $\overrightarrow{U_d}$. Equation of transport of a UDS (ϕ_k) s in general form is as follows [4]:

$$\frac{\partial \rho \phi_k}{\partial t} + \nabla \cdot \left(\vec{\psi}\phi_k - \Gamma_k \cdot \phi_k\right) = S_{\phi k}. \tag{4}$$

In the implemented model, according to equations (1) and (2) the advection vector $\vec{\psi}$ was equal to $\rho_d \overrightarrow{U_d}$ and the dissipation coefficient was set to zero. The right-hand term was defined for each scalar according to equations (1) and (2). In the solutions of these equation the assumption of one-way coupling of the phase motion was assumed, i.e. that air flow influences flow of dispersed water phase and is not influenced by it. This assumption is commonly used in publications of similar works because of volume ratio of air and dispersed water phases approaching unity. In the presented here examples ρ_d was set to 1.9 g/m^3, typical for atmospheric strati form clouds, which makes volume ratio of the phases equal to 0.99981.

Apart from implementation of transport equations for variables representing flow of dispersed water the solid-wall boundary condition on the object surface (e.g. aircraft wing) requires special

treatment [1]. In order to speed-up convergence and avoid unphysical solution the sign of the term $\vec{n} \cdot \vec{U}_d$, where $\vec{n}$ is surface normal vector, is computed along the object surface. If the sign of this dot product is negative, the local value of ρ_d on the surface is set to zero. In the opposite case this value is set equal to value in the centre of computational cell and may be used for determination of local value of water mass hitting the surface in unit time.

3. Strategy of solution of flow equations and obtained solutions

Conditions of interest for aerodynamics and aircraft design in applications of the flow model include wide range of Mach numbers and angle of attack, from low values to high values, close to maximum lift, which represent conditions typical for landing approach, especially on extended flap surfaces. In such conditions, there appear regions of reversed flow, due to flow separation on the rear part of the wing section, shown in Fig. 1 with dark colour. In general case, due to different inertia of air and water, the boundaries of these zones for both phases do not coincide, and the solution for water-phase flow converges after the solution of air flow has converged. In the process of obtaining the solution in the area of flow recirculation, the solution is susceptible to divergence in cells, such as presented in the right-hand side of Fig. 1, where the dispersed water is entering computational cell from two sides: from front with the mainstream flow and from the rear side with recirculated flow. In such scenario, the density ρ_d is likely to rise, due to mass conservation equation, and then the force $\vec{f}_d$ rises too as a consequence of rising ρ_d. In order to avoid divergence, the solution has to be conducted using unsteady solver, which guarantees the same time step in the whole computational domain. In these flow conditions, low enough time step, below 0.001s, has to be applied with low under-relaxation coefficients. With such solution parameters flow of dispersed water assumes the general pattern of airflow and changes direction in the cell shown in Fig. 1 such that water is transported upwards and the solution converges to a steady-state flow parameters.

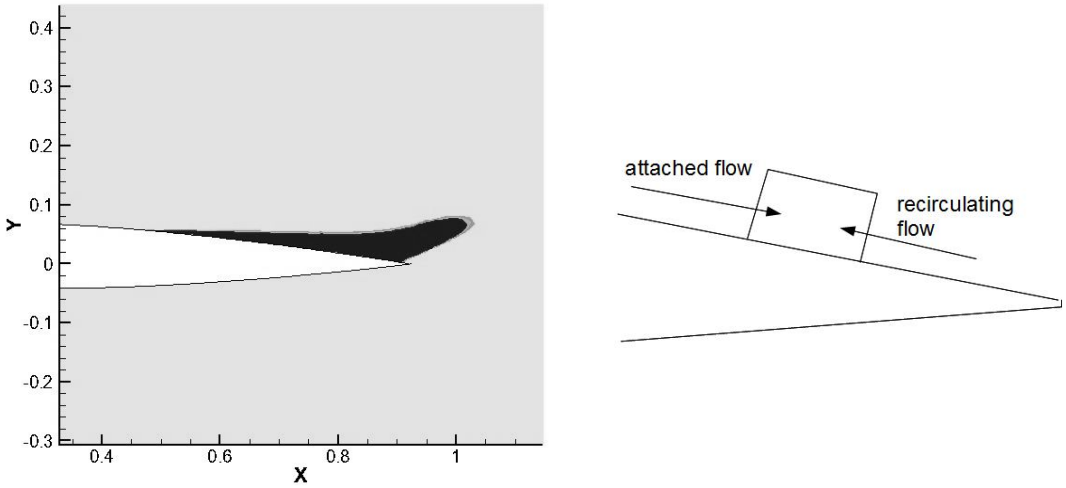

Fig. 1. Left side: contour of negative X-velocity (recirculating flow- dark grey) at high-angle-of-attack flow, right side: flow pattern in computational cells where divergence of the solution has to be avoided

An indication of the process of convergence of the unsteady solution of the two-phase flow in time is convergence of the nondimensional coefficient of water collection in a surface point defined in equation (5). Convergence of this coefficient in the stagnation point at airfoil leading-edge, where water collection is maximum is shown in Fig. 2.

$$\beta = \frac{\rho_d \vec{V}_d \cdot \vec{n}}{\rho_{d\,inf} \cdot \vec{V}_{inf}}. \tag{5}$$

The converged solution for β in the stagnation point, obtained using the presented procedure, compared with experimental results presented in [1] for NACA 23012 airfoil is shown in Fig. 3. Flow conditions in this test solutions were Mach number Ma-0.22 and angle of attack α=2.5°. In the left part of Fig. 3 is presented comparison of the distribution along airfoil perimeter of the coefficient β computed using the described above procedure with results of experiment at α=2.5° and on the right part of this figure is presented comparison of computed distributions of β at 2.5° and 14°. The "s" coordinate is measured along the airfoil perimeter with zero in the stagnation point (maximum static pressure). It can be seen that maximum value of β is well predicted with the computational method and differences between computed and measured values occur mainly near the borders of the wetted area. According to the literature, the main reason for this is approximation of the spherical shape of the droplets, which in reality deform near the object and assume different trajectory due to changes of aerodynamic forces. As the angle of attack increases to 14° the width of the wetted area increases too with decrease of the peak value of β. It can also be seen that at α=14° in the area of reversed flow on upper surface, where "s" is close to unity water is not hitting the surface.

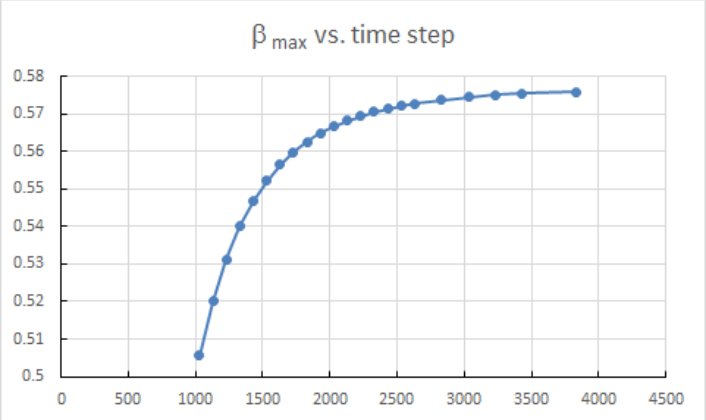

Fig. 2. Convergence of the coefficient of water collection β in the stagnation point at airfoil leading edge

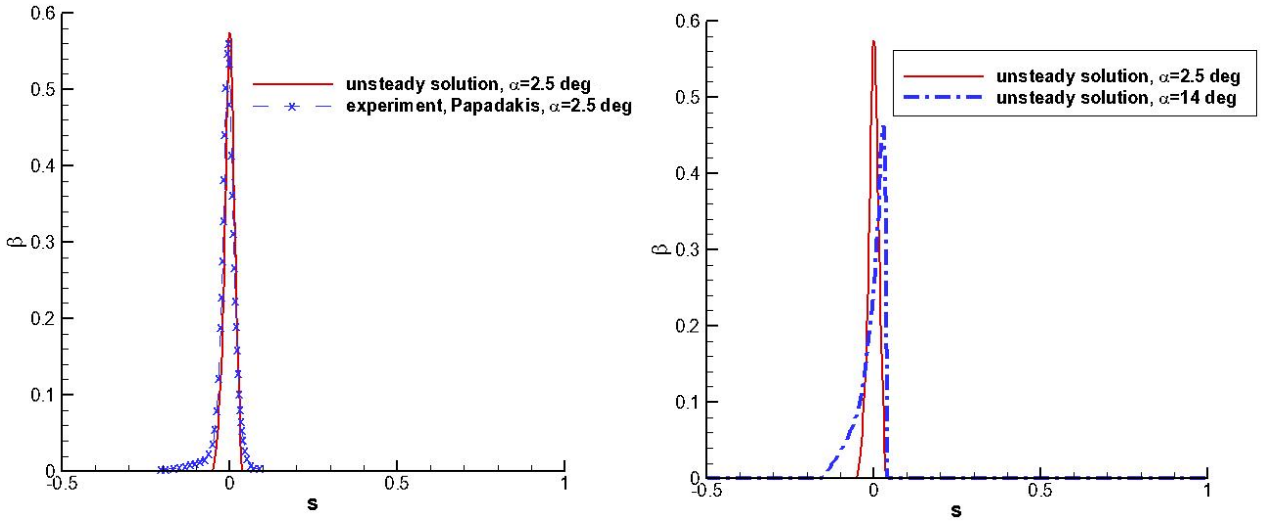

Fig. 3. Comparison of the of the distribution of β coefficient along airfoil chord obtained from unsteady numerical solution at Ma=0.22, α=2.5° with results of experiment (left) and comparison of the distributions of β coefficient obtained from unsteady computations at α=2.5° and α=14°

From the point of view of effectiveness of the computational method, any possibility of reduction of the computational zone for the solution of the dispersed-water phase is highly valuable. The computational zone for air flow must be much larger than the investigated object;

boundary conditions have to be imposed at least 10 characteristic dimensions in each direction from the object so that pressure and velocity non-uniformities created by the object do not reach the boundaries where uniform flow is assumed. On the other hand, if the problem modelled is flight through stationary atmosphere, then some distance upstream from the object both air and dispersed water are stationary. The incoherencies of the velocities of both phases can be captured by evaluating their dot product and dividing by product of their modules, which is shown in Fig. 4. It can be seen that for converged solution the incoherencies between local phase velocities disappear and their dot product approaches unity approximately one chord upstream and in both vertical directions from the airfoil surface. For this reason a hypothesis of the possibility of limitation of computational zone for the dispersed water was tested, which was limited by a distance from its surface of approximately twice the characteristic dimension of the object. The limited zone is shown in Fig. 5 as circular sub-region of the computational mesh.

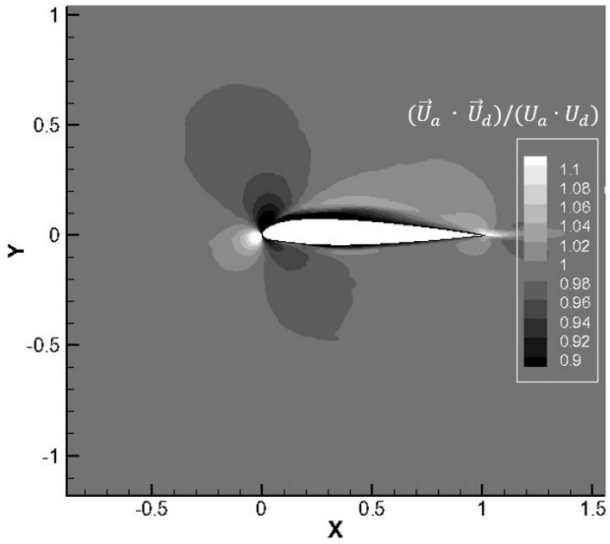

Fig. 4. Contour of dot product of air- and dispersed water velocities in the vicinity of NACA 23012 airfoil

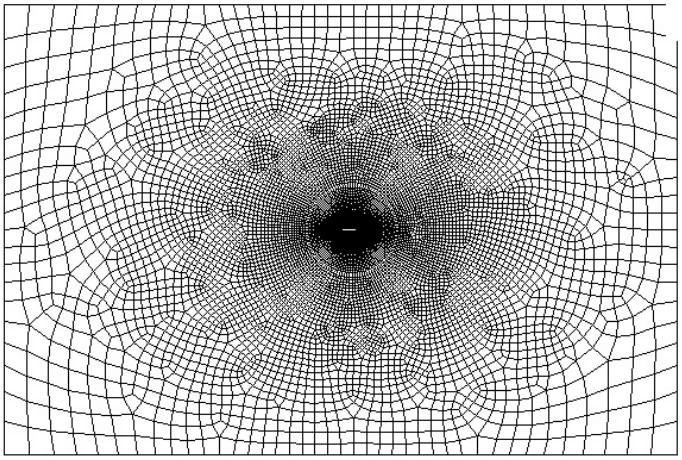

Fig. 5. Schematic view of the computational domain with internal sub-domain visible as limited by white circle to which solution of the transport equations of the dispersed water phase was narrowed

The computations of the flow of dispersed-water phase in the internal sub-domain were started after the solution for air flow has converged. This, consistent with the assumption of one-way coupling between phases, made it possible to "freeze" the air flow and solve only the equations for variables of the second phase. On the boundary of the sub-zone the "outlet" boundary condition was applied which had no impact on the "frozen" air flow but allowed for setting of constant mass-

flow rate of the secondary phase. The results of the computations in terms of the contour of ρ_d with enlarged region of its non-uniformity, and comparison of the β coefficient computed in large and small domain are shown in Fig. 6.

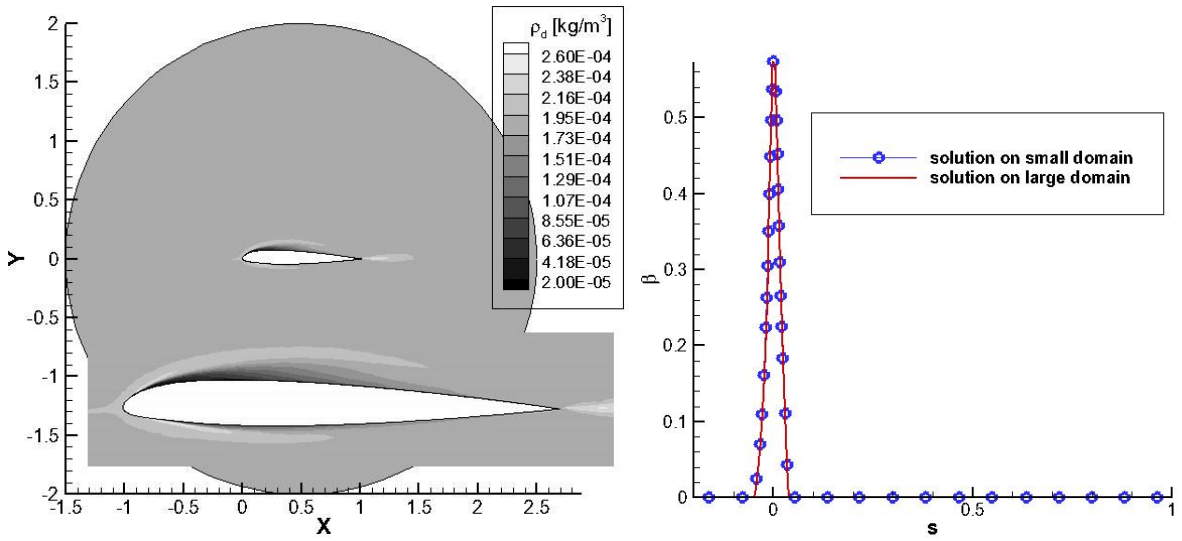

Fig. 6. Left side: Contour of density of the dispersed water phase ρ_d in the vicinity of NACA 23012 airfoil obtained in the internal sub-domain of mesh presented in Fig. 5 with enlarged fragment of non-uniformities near airfoil surface . Right side: comparison of surface distribution of β coefficient computed with equations of transport of the dispersed-water phase solved in large and narrowed domain

The presented two-phase flow computational model is not restricted to two-dimensional flow cases. A three-dimensional case was created based on computational mesh used for determination of aerodynamic loads acting on modified tail-rotor blade of Mi-2 helicopter, shown in Fig. 7, being a part of a bigger mesh for the solution of airflow. The solution for dispersed water phase, in terms surface distribution of mass of water hitting blade surface is shown as surface contour in Fig. 8, where a distinctive zone of water hitting the surface is visible as a light band at the blade leading edge, getting wider towards blade tip.

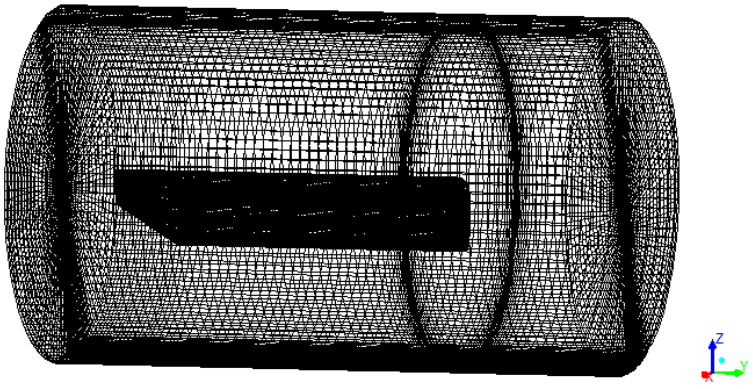

Fig. 7. Computational zone for solution of dispersed-water flow around helicopter tail-rotor blade

Although a direct comparison with experimental data was not possible in this case, a qualitative verification was possible. In the paper [5] results of icing wind-tunnel experiment were presented, as cross-sectional shapes of ice deposits at the leading edge in several equidistant sections of the blade span. Areas of these cross-sections of ice deposits, proportional to mass rate of water hitting the blade surface, were evaluated and are presented in Fig. 9, showing similar tendency of rise of mass of water hitting blade surface along its span.

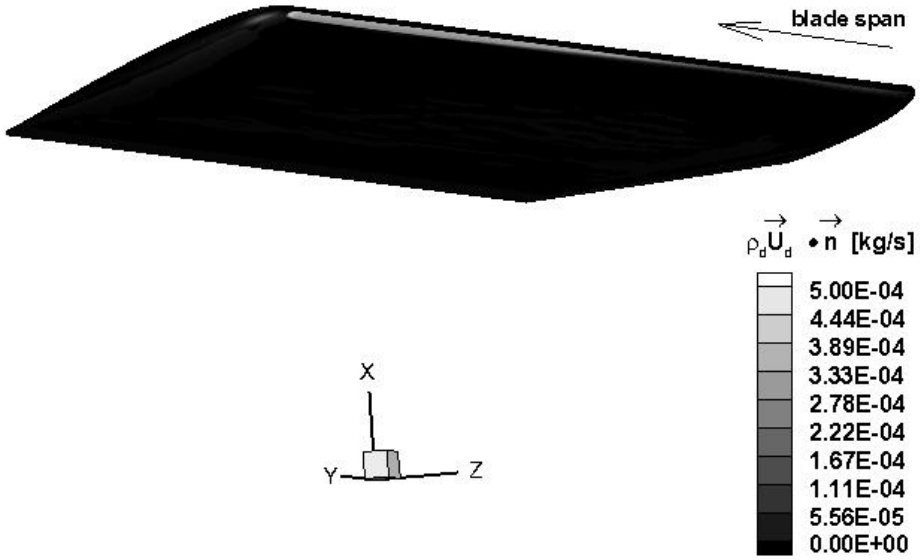

Fig. 8. Contour of surface distribution of mass of water hitting blade surface

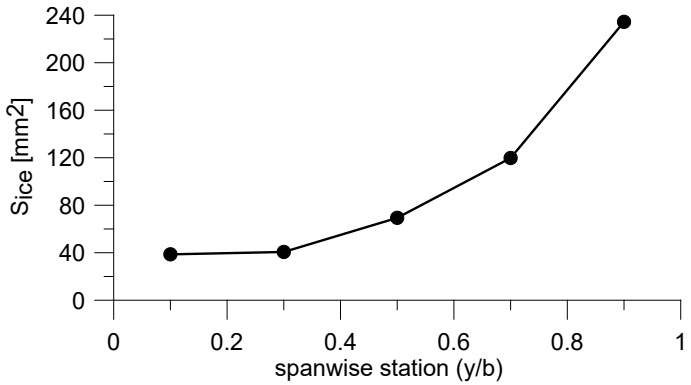

Fig. 9. Results of experiment in icing wind tunnel showing span wise distribution of accreted ice [5]

4. Conclusions and future work

Assumption of one-way coupling between motion of phases in a dilute two-phase flow, applied in conditions of dispersed water in atmospheric clouds allows for separation of the computational processes of obtaining a solution for problems of water depositing on aerodynamic surfaces, including limitations of the size of the domain for the solution of motion of the dispersed-water phase to the length of several characteristic dimensions of the object under analysis in upstream and downstream direction. Boundary conditions for the secondary phase applied on the boundaries of the internal computational zone should ensure uniformity of the density of dispersed water and coherence of air and water-droplet velocities in the boundary surface upstream of the object. The computational model presented in this paper is under development and its intended functionality assumes possibility of conducting simulations of the accretion of ice and its effect on aerodynamic characteristics of the elements of aircraft critical to flight safety: lifting and control surfaces, engine inlets, sensors of flight parameters.

References

[1] Hospers, J. M., Hoeijmakers, H. W. M., *Numerical Simulation of SLD Ice Accretions*, Proceedings of the 27th International Congress of the Aeronautical Sciences, 2010.

[2] Beaugendre, H., Morency, F., Habashi, W.G., *FESNSAP-ICE's Three-Dimensional In-Flight Ice Accretion Module: ICE3D*, Journal of Aircraft, Vol. 40, No. 2 2003.

[3] Morrison, F. A., *Data Correlation for Drag Coefficient for Sphere*, Department of Chemical Engineering, Michigan Technological University, Houghton, MI, *www.chem.mtu.edu/ /~fmorriso/DataCorrelationForSphereDrag2010.pdf.*
[4] ANSYS FLUENT UDF Manual, ANSYS, Inc. Southpointe 275, Technology Drive Canonsburg, PA 15317.
[5] Fortin, G., Perron, J., *Spinning Rotor Blade Tests in Icing Wind Tunnel*, 1st AIAA Atmospheric and Space Environments Conference, AIAA 2009-4260, San Antonio, Texas 22-25 June 2009.